Chemical Geology 638 (2023) 121694

Contents lists available at ScienceDirect

Chemical Geology

journal homepage: www.elsevier.com/locate/chemgeo

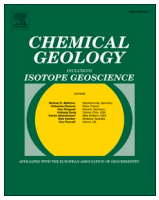

Obsidian clasts as sintered remnants of agglutination processes in volcanic conduits, evidence from the Pepom tephras (Sete Cidades), São Miguel, Azores

B.S. Ellis [a,*], A. Pimentel [b,c], E.A. Cortes-Calderon [a], Z. Moser [a], N. Baumann [d], O. Bachmann [a], F.B. Wadsworth [e]

[a] Institute of Geochemistry and Petrology, ETH Zürich, 8092 Zurich, Switzerland
[b] Instituto de Investigação em Vulcanologia e Avaliação de Riscos (IVAR), Universidade dos Açores, 9500-321 Ponta Delgada, Portugal
[c] Centro de Informação e Vigilância Sismovulcânica dos Açores (CIVISA), 9500-321 Ponta Delgada, Portugal
[d] Friedrich-Alexander-Universität Erlangen-Nürnberg, GeoZentrum Nordbayern, Schlossgarten 5, 91054 Erlangen, Germany
[e] Department of Earth Sciences, Durham University, Durham DH1 3LE, UK

ARTICLE INFO

Editor: Dr. Claudia Romano

Keywords:
Obsidian
Sintering
Trachyte
Azores
Geochemistry

ABSTRACT

The youngest explosive eruptions of the Sete Cidades volcano, São Miguel, Azores, are recorded by a series of relatively small-volume (<0.03 to 0.13 km^3 DRE) trachytic pyroclastic deposits termed the Pepom tephra deposits. While dominated by crystal-poor to crystal-moderate (<10%) pumice clasts, these deposits also contain a suite of dense glassy clasts of broadly similar crystallinity. The obsidian clasts from a single deposit vary in texture from entirely dense to those that are moderately vesicular and typically single clasts will contain multiple textural domains. The majority (~71%) of these dense clasts have compositions both from bulk rock and in-situ glass measurements that are identical to those of the pumice clasts within the same deposit. We interpret these dense clasts to reflect sintering of previously fragmented magma at shallow levels in the conduit prior to being re-entrained and erupted with the vesicular magma, in agreement with recent studies focussing on textural observations. Notably, across the exposed volcanic stratigraphy of São Miguel obsidian domes, flows/coulees are not preserved, arguing against the idea that the dense glass clasts within the Pepom tephras are sourced from existing surficial rocks. In contrast, the neighbouring island of Terceira exhibits domes and coulees with large obsidian bands that cut through the crystalline groundmass. Most silicic rocks of Santa Bárbara and Pico Alto volcanoes on Terceira are peralkaline, comenditic to pantelleritic in composition, and at similar conditions (e.g., temperature and water content) have lower viscosities than the trachytic Pepom obsidian clasts. However, the Santa Bárbara silicic lavas on Terceira (the less peralkaline suite) have more obsidian than the more peralkaline Pico Alto domes and coulees indicating that while peralkalinity, developed during magmatic evolution in the crust, may play a role, sintering occurring at shallow levels within the conduit likely is more important in producing obsidian.

1. Introduction

Pyroclastic deposits commonly contain a variety of clasts, from those that are evidently the remains of the magma that drove the eruption (i.e. juveniles) to a range of incorporated lithologies commonly termed lithics. Magmatic petrology primarily focuses on the juvenile component of the deposits to understand the pre-eruptive physico-chemical conditions of the magmatic plumbing system. The lithic clasts, however, may provide important information about a variety of facets of the system and are increasingly being exploited as an additional information source. Mantle xenoliths containing fluid inclusions, intrusive or pseudo-intrusive clasts can reveal details about the rinds of the magmatic system - particularly in young volcanic suites where erosion is insufficiently progressed to expose intrusive lithologies (e.g. Hansteen et al., 1998; Bachmann et al., 2007; Pittari et al., 2008). Dense, glassy clasts varying from obsidian to vitrophyric in nature are a common feature of many pyroclastic deposits from around the world (e.g., Hildreth and Mahood, 1986; Rust et al., 2004; Rust and Cashman, 2007;

* Corresponding author.
E-mail address: ben.ellis@erdw.ethz.ch (B.S. Ellis).

https://doi.org/10.1016/j.chemgeo.2023.121694
Received 26 May 2023; Received in revised form 18 August 2023; Accepted 25 August 2023
Available online 26 August 2023

Gertisser et al., 2010, amongst many). Where juvenile, such obsidians are thought to be formed within the shallow levels of the conduit through repeated cycles of fragmentation and sintering (Gardner et al., 2017; Watkins et al., 2017; Wang et al., 2021). Obsidian bombs and lavas may contain tuffisite veins (e.g., Castro et al., 2014; Tuffen et al., 2022) recording periodic brittle behaviour. Obsidian compositions, and particularly their volatile contents (e.g., H_2O, CO_2, S species etc.), have been used to shed light on degassing behaviour (Taylor et al., 1983; Newman et al., 1988; Barnes et al., 2014) and the complex transitions between explosivity and effusion observed in recent eruptions (Wadsworth et al., 2020; Schipper et al., 2021). Where the obsidian clasts can be shown to be lithic (e.g., Wilson and Hildreth, 1997), they have the potential to reveal information about the subsurface geology and volcanic stratigraphy that may otherwise be inaccessible and allow a more complete eruptive history of the volcano to be unravelled. A fundamental difficulty in many pyroclastic deposits is to establish whether or not an obsidian clast is genetically related to the vesicular magma with which it was co-erupted. With physical features of the obsidians resulting from multiple generations of overprinting processes (i.e. repeated cycles of fragmentation and sintering), an alternative method to constrain their origin is the geochemistry of the melt phase (e.g., Monnereau et al., 2021). In this study, we employ a geochemical approach to understanding the origin of the obsidian cargo in young pyroclastic deposits of the Sete Cidades volcano, São Miguel, Azores.

2. Sete Cidades volcano

Volcanism in the Azores region is thought to be the result of interaction between a deep melting anomaly (often referred to as the Azores hotspot) and the triple junction of the North American, Eurasian and Nubian lithospheric plates. The nature of this interaction has been the subject of numerous studies (Cannat et al., 1999; Turner et al., 2007; Beier et al., 2012; Métrich et al., 2014; Trippanera et al., 2014, amongst others). The Sete Cidades volcano is the westernmost of the three active central volcanoes on the island of São Miguel and is crossed by the tectonic structures of the ultraslow-spreading Terceira Rift (Vogt and Jung, 2004; Carmo et al., 2015, Fig. 1). Like the two other active central volcanoes of São Miguel (Fogo and Furnas), Sete Cidades hosts a summit caldera (approximately 5 km wide) that encloses perennial lakes infilling volcanic craters.

The volcanic stratigraphy of Sete Cidades is split into the Inferior Group that consists of the deposits of older (>36 ka to as old as 210 ka; Moore, 1990) volcanic activity and the Superior Group that contains the younger deposits (Queiroz, 1997; Queiroz et al., 2015) including the three major pyroclastic formations of Risco (35,740 ± 810 ^{14}C yr BP), Bretanha (28,750 ± 240 ^{14}C yr BP) and Santa Bárbara (15,740 ± 200 ^{14}C yr BP). The Santa Bárbara Formation (0.25–0.54 km^3 DRE) records the last stage of caldera-widening at Sete Cidades (Porreca et al., 2018; Kueppers et al., 2019; Laeger et al., 2019). After this paroxysmal event, a diverse array of activity is recorded by the Cascalho Negro Member (16 ka to ~5 ka), prior to the Pepom Member that is composed of trachytic tephra deposits intercalated with subordinate basaltic scoriae and lavas

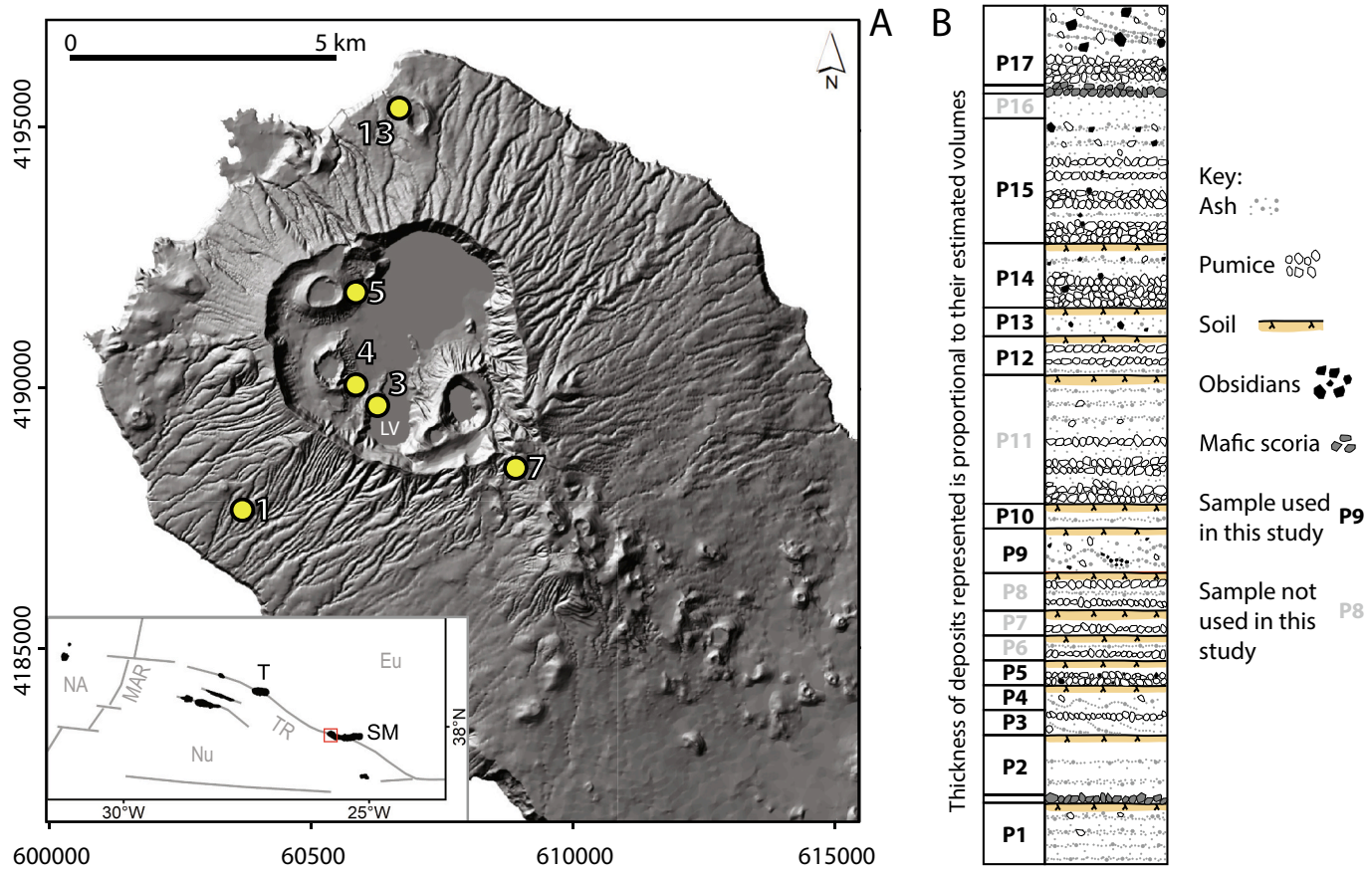

Fig. 1. The Sete Cidades volcano and Pepom tephra deposits (modified after Ellis et al., 2022). A. Digital elevation model (DEM) of Sete Cidades with sampling locations (commonly following Queiroz, 1997) illustrated by yellow circles (LV – Lake Verde). Inset shows the location of São Miguel (SM) and Terceira (T) islands in the Azores archipelago and the main tectonic features of the region (Eu – Eurasian plate, Nu – Nubian plate, NA – North American plate, MAR – Mid-Atlantic Ridge, TR – Terceira Rift). Small red box represents the location of Sete Cidades. B. Generalised vertical stratigraphy (GVS) of the Pepom tephra deposits after Ellis et al. (2022) with thickness proportional to estimated eruptive volume (Queiroz et al., 2008, 2015). Deposit names in black illustrate data presented in this study. (For interpretation of the references to colour in this figure legend, the reader is referred to the web version of this article.)

erupted from vents on the flanks of Sete Cidades (Queiroz et al., 2008, 2015).

The Pepom tephras are amongst the youngest volcanic products on São Miguel and are temporally constrained by overlying the Fogo A deposit (4.6 ka) and preceding the arrival of the Portuguese in the 15th century. These tephras were erupted from a series of vents that are variably exposed within the caldera today. These intra-caldera eruptions were relatively small in volume (<0.03 to 0.13 km^3 DRE, Queiroz et al., 2008) and produced fall and non-welded pyroclastic density current deposits (Cole et al., 2008; Queiroz et al., 2008). All 17 Pepom tephras are trachytic in composition (SiO_2 62.9–65.5 wt%) and crystal-poor to crystal-moderate with alkaline feldspar (mostly sanidine and anorthoclase) as the dominant mineral phase. Additional phases include biotite, clinopyroxene, apatite, Fe—Ti oxides and rare amphibole (Ellis et al., 2022). The eruptions that gave rise to the Pepom tephra deposits were predominantly hydromagmatic, with some alternating between magmatic and hydromagmatic phases within the same event. In addition to the vesicular, pumiceous products of the eruptions, dense glassy clasts are near-ubiquitous in these deposits (Queiroz et al., 2008; Ellis et al., 2022). These obsidian clasts are the subject of this work.

An interesting feature of the Sete Cidades volcano is how little of the post-caldera record (after the 16 ka Santa Bárbara eruption) involves effusive silicic volcanism, despite effusive eruptions being frequent at many other calderas, like at the neighbouring Furnas volcano (Guest et al., 1999), or at Pico Alto and Santa Bárbara volcanoes on Terceira Island (Self, 1976), amongst other examples worldwide. At Sete Cidades the volcanism sourced from the caldera system in the last 16 ka has been predominantly explosive (i.e. excluding the occasional 'leaks' of magmas from lateral vents, recorded by a few basaltic and trachytic lavas of the Cascalho Negro and Pepom members), where glassy fragments are not observed. Here, we texturally and geochemically investigate the compositions of the obsidian clasts co-erupted with the Pepom tephras to distinguish between them resulting from within-conduit processes or from external sources.

3. Methods

Individual obsidian clasts were sampled from within 12 of the 17 Pepom tephra deposits (as sampled by Ellis et al., 2022; Fig. 1, sample locations in supplementary material). The smaller clasts were cleaned and mounted in 1-inch round epoxy mounts and polished for in-situ imaging and major and trace element geochemical analyses. Larger clasts were variably sub-split to produce material for X-ray fluorescence (XRF) analysis as well as to make thin sections for textural observations and micro-analysis. All analytical work was carried out within the Institute of Geochemistry and Petrology, ETH Zurich.

3.1. Imagery

Obsidian textures were observed using a petrographic microscope on thin sectioned pieces from the larger clasts and a JEOL JSM-6390 scanning electron microscope (SEM) on the smaller pieces. Qualitative and quantitative major element mapping of such clasts was also performed using a JEOL JXA-8230 electron microprobe. Maps were acquired at 15 kV and 100 nA, using a focused beam and acquisition time of 100 ms. Quantitative maps were obtained with Probe-image and processed using Calc-image softwares (Donovan et al., 2018)

3.2. Bulk rock geochemistry

Samples for bulk geochemical analysis were prepared and analysed in a standard manner. Following overnight drying, for each sample 1.5 g of powder was heated to 850 °C to determine the loss on ignition (LOI). After re-grinding, the sample was then mixed with a lithium tetraborate flux at a ratio of 5:1, flux:sample. A 2.4 kW PANalytical Axios wavelength-dispersive X-ray-spectrometer was employed for analysis. The glass beads were subsequently broken and interior portions analysed via LA-ICPMS for trace and rare earth elements using a 193-nm Lambda-Physik excimer ArF-laser coupled to a PerkinElmer-ELAN-6100 ICP-MS system following procedures in Troch et al. (2018).

3.3. In-situ major element analyses

Microprobe analyses of glasses from the dense, glassy clasts followed identical procedures to those outlined in Ellis et al. (2022) thus allowing ready comparison between the dense obsidians and the vesicular pumice clasts from the Pepom tephras. In brief, glasses were measured with a 5 spectrometer JEOL JXA-8230 electron microprobe. Operating conditions were beam energy of 15 keV, beam current of 10 nA, and the beam diameter of 20 μm. Analysis of Na and K was first to ensure minimal alkali migration and, if necessary, a time dependent intensity correction was applied. On-peak counting times were between 20 and 40 s for all elements, with the exception of F that was acquired for 60 s. We undertook stability tests of the glass before acquiring the unknowns to ensure appropriate counting times and beam conditions. The mean atomic number background intensity data were calibrated, and continuum absorption corrected for all elements (Donovan and Tingle, 1996; Donovan et al., 2016). Deadtime corrections were applied to all unknown and standard intensities and standards were drift corrected if required. We applied a Phi-Rho-Z matrix correction algorithm with the Chantler's FFAST X-Ray Form Factor, Attenuation, and Scattering Tables (NIST v 2.1, 2005) dataset used for calculations and mass absorption coefficients. Probe for EPMA (Donovan et al., 2018) was used to collect and process the data.

3.4. In-situ trace element analyses

Concentrations of trace elements in glasses, were determined by LA-ICPMS using a 193 nm Resonetics ArF excimer laser coupled to a Thermo Element XR ICPMS. Spot analyses were mostly between 29 and 43 μm with a laser output energy of c. 3.5 J/ cm^2. NIST612 and additional reference glass GSD-1G were measured after every 25 to 30 unknowns to monitor for drift. The MATLAB-based program SILLS (Guillong et al., 2008) was used for data reduction, with microprobe measurements used for internal standardisation. Long-term analysis of reference material reproducibility indicates that precisions are typically better than 5% relative when abundances are comfortably (3× or more) above limits of detection.

All new data for this study and measurements of reference materials are provided in supplementary materials.

4. Results

4.1. Textures of obsidian clasts

Pepom obsidian clasts are most commonly observed as dark green to black, centimetre-scale angular to sub-angular fragments with the largest clasts reaching 10–15 cm in diameter. After cleaning, the largest clasts display lighter coloured, more vesicular veins cutting through the dense dark green to black glass (Fig. 2).

These vesicular zones are typically on the centimetre-scale and have sharp boundaries to the surrounding dense glass. On a finer scale, the obsidians exhibit strong textural variability within a single clast or thin section (Fig. 3, Sup. Fig. 1). A commonly occurring feature is that of a more vesicular zone with abundant groundmass crystallisation, often juxtaposed with zones of dense glass (Fig. 3). In a number of cases these microcrystalline portions are both more vesicular and contain large (mm-scale) crystals. Throughout all the obsidians studied here the predominant groundmass mineral phase is feldspar, typically found in strongly elongated crystal shapes. The obsidian vesicularity is highly variable. Some clasts are entirely dense while others are extremely vesicular. The shapes of the vesicles themselves may be elongate with

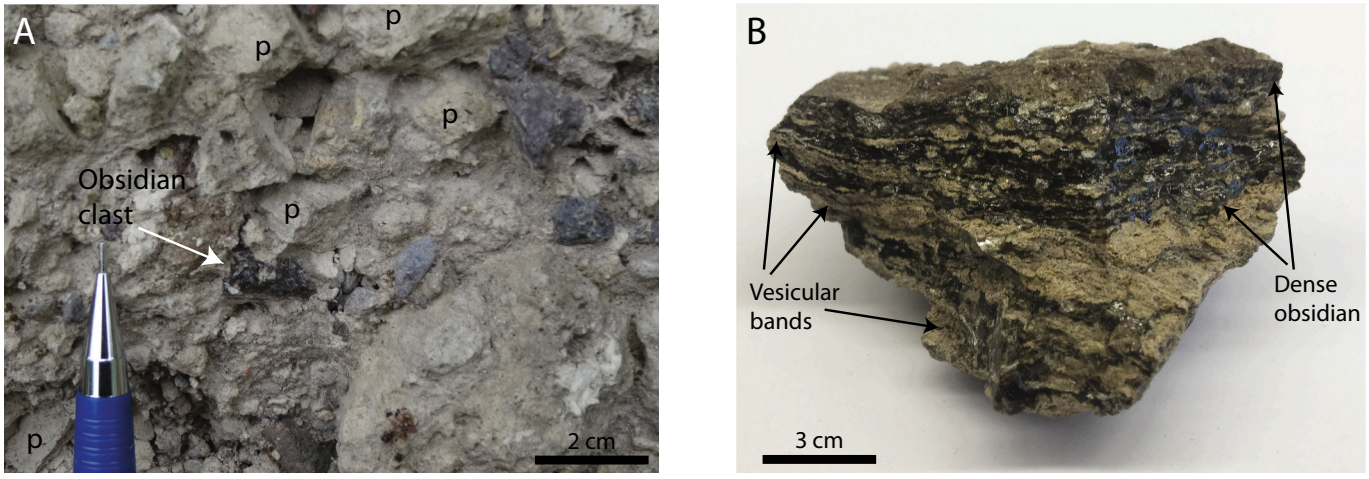

Fig. 2. Appearance of Pepom obsidian clasts. A. Small obsidian clast in the P15 tephra deposits, p reflects pumice clasts in the same deposit. B. Larger obsidian clast (10 cm diameter) from P13 following cleaning to highlight the lighter coloured bands running through the clast.

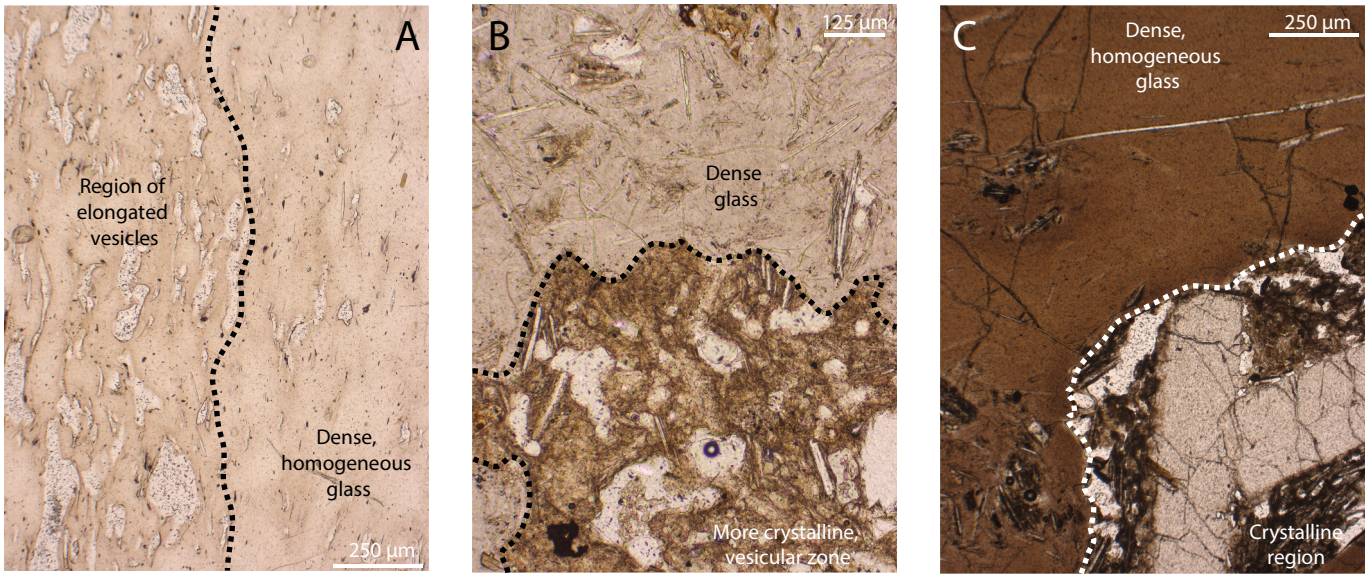

Fig. 3. Appearance of the obsidian clasts in thin section. A. Elongated vesicles in the left hand side of the image with dense, homogeneous glass in the other indicating different histories for neighbouring portions of the same P17 obsidian clast. B. Contrasting groundmass textures within a P13 obsidian with dense glass at the top and more crystalline groundmass with larger bubbles in the lower portion of the image. C. Another P13 obsidian with differing glass domains where the large crystals are related to the more microcrystalline, vesicular groundmass.

pointed ends, near-equant (in 2 dimensions) or deformed (a library of obsidian textures is provided in supplementary material 1). Dense clasts in the P11 deposit are almost entirely devitrified and fully crystalline (Sup. Fig. 1) and so their compositions are not considered here.

Electron microprobe compositional maps show that the dense portions of the obsidians can be observed to be compositionally homogeneous (sup. Fig. 2) while the small crystal phases elevated Na and K and depletion in Fe that are consistent with the textural observation of feldspar being the dominant groundmass phase.

4.2. Bulk rock geochemistry

The vesicular components (pumice) of the Pepom tephra deposits are exclusively trachytic, with some of the earlier erupted deposits (P2-P5) being slightly less evolved than the rest of the suite (as shown by Ellis et al., 2022). Proximally, the P13 and P15 deposits have obsidian clasts that are sufficiently large to allow for bulk rock geochemistry. While in both deposits the major elemental compositions of the obsidians are roughly similar (Figs. 4B and 5), the trace elemental compositions are quite different, highlighting the power of elements that have large partition coefficients in the extant mineralogy to reveal processes. In the case of P13, the compositional agreement between the obsidians and the pumiceous clasts found within the same deposits is remarkable (Fig. 4C). Comparing the average bulk rock compositions of pumices ($n = 3$) and obsidians ($n = 6$) across all trace elements returns a near-perfect correlation ($R^2 = 0.9995$), supporting the idea that the obsidian and pumice clasts within this deposit are genetically related. In contrast, in P15 the obsidians have rather different compositions. One obsidian (obsidian 4 in Fig. 4D) has a similar composition to the P15 pumice and could be produced in the same way as the P13 obsidians. Three others (Fig. 4D) however have distinct compositions that require alternative explanation.

4.3. In-situ geochemistry

Smaller (typically cm-scale) obsidian clasts are found in many of the

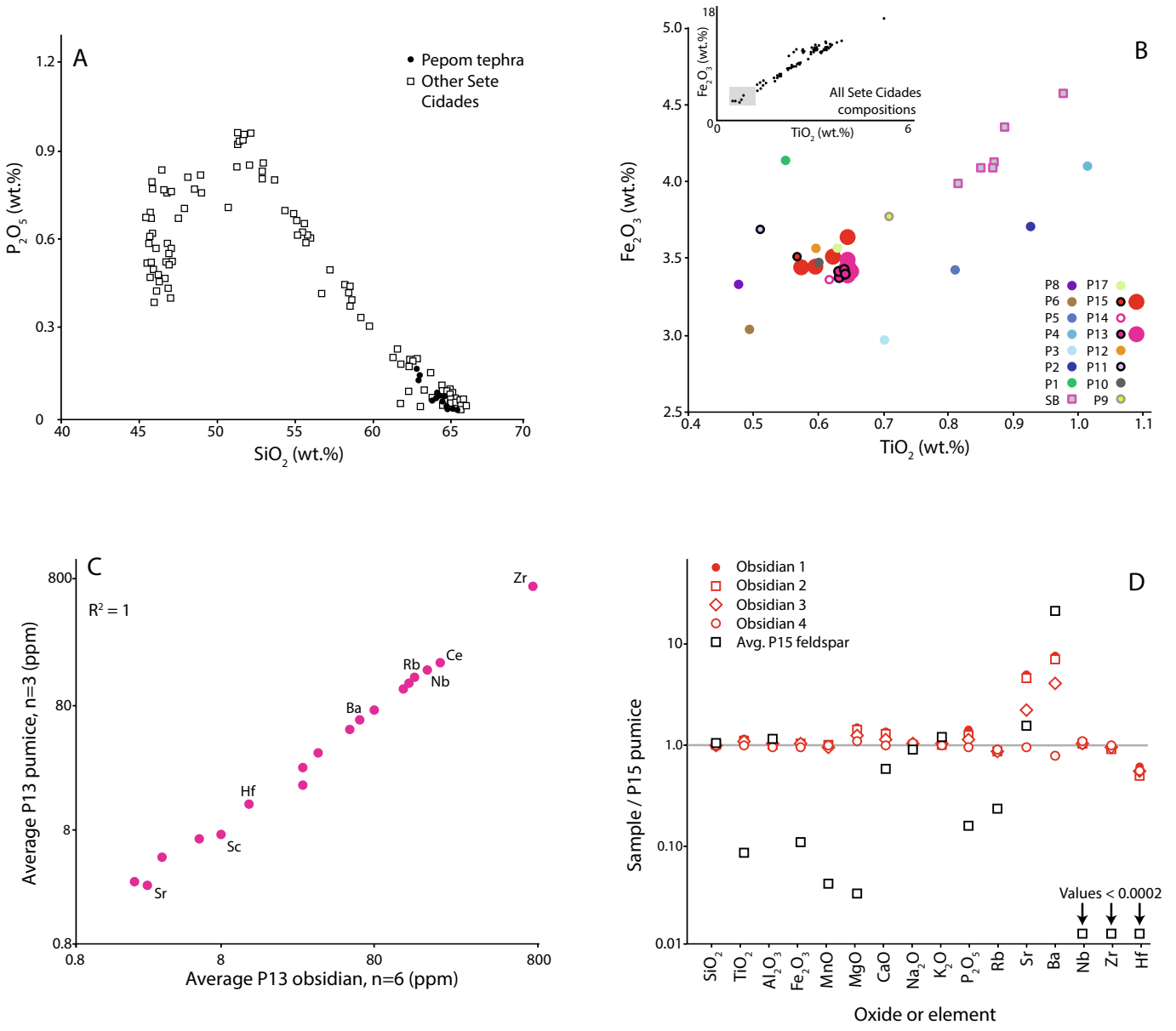

Fig. 4. Bulk rock compositions of the obsidian clasts. A. Overall compositional range for the Sete Cidades volcano (data from Beier et al., 2006; Ellis et al., 2022) with the most evolved samples, used in this study, highlighted. B. The large obsidian clasts in the P13 deposits (large symbols) have major elemental compositions that are a good match for the bulk pumices (smaller symbols, Ellis et al., 2022) of the P13 deposits while P15 obsidians show little overlap with bulk pumices. The whole range of erupted compositions reported by Beier et al. (2006) for Sete Cidades are shown in the inset. SB represents the Santa Bárbara deposits that were the last caldera modifying eruption at Sete Cidades. C. Average trace element composition of pumices and obsidians in P13 showing an almost perfect correlation indicating a common source. D. Bulk compositions of obsidian clasts within P15 compared to the P15 pumice composition. Also shown is the average P15 feldspar composition (Ellis et al., 2022) illustrating that the compositions of obsidians 1–3 in the P15 deposit cannot be explained by feldspar accumulation.

Pepom tephras (e.g., Figs. 1, 2) and these were utilised for in-situ geochemistry. For these clasts, to simplify the large amount of data, we plot the average compositions of the 60 obsidian clasts that we investigated (all individual analyses available in supplementary materials). The analytical totals of the 178 analyses averaged 98.72 wt% and variability in Na_2O/K_2O ratio shows little relationship with analytical total indicating that the obsidians have not experienced significant post-eruption hydration. In the P2-P5 package of units the obsidians contain notably more CaO (mostly above 0.8 wt%) than the other Pepom tephra deposits (typically around 0.5 wt%, Fig. 5B). This is a similar result to that found for the pumice glasses of the Pepom deposits presented by Ellis et al. (2022). In other respects, the obsidian clasts have rather similar major elemental chemistry. Trace elements are considerably more informative than major elements in terms of distinguishing the origin of the dense clasts (Fig. 6) as a result of the large dynamic range of compositions (for example Ba varies by two orders of magnitude across different obsidian clasts). Overall, the obsidian clasts follow the behaviour of the groundmass glass compositions (Ellis et al., 2022) with the P2-P5 package distinguished by higher V, Ba, Sr, and lower La and Ce than the rest of the Pepom tephras. Similarly these less evolved P2-P5 tephras have a notably higher Eu/Eu* between 0.69 and 1.09 compared to the typical Pepom values of 0.5 and 0.65. Some clasts in P1 and P17 have compositions similar to this P2-P5 package. In the case of P17, this is readily explainable as entrainment of existing material, however in the case of P1 (stratigraphically beneath the P2-P5 package) this explanation does not hold. This suggests that there may be additional obsidian sources within the shallow subsurface that remain unknown.

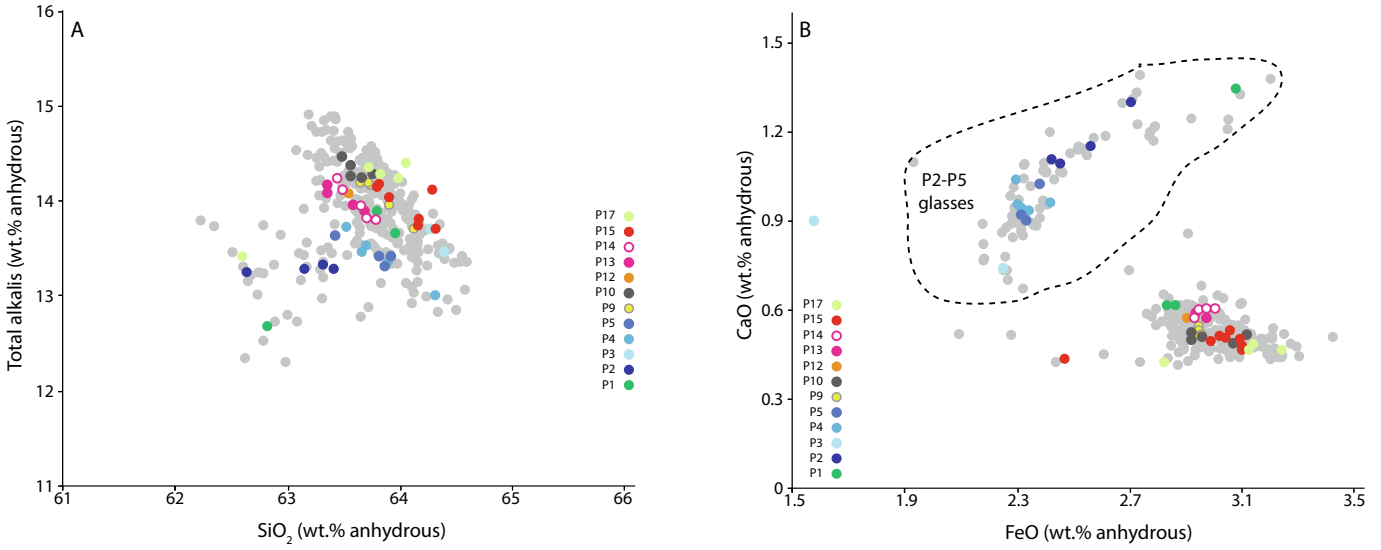

Fig. 5. Major elemental compositions of the obsidian clasts compared to the vesicular glasses of the Pepom tephra deposits from Ellis et al. (2022) shown as grey circles. A. In major elemental space, almost all of the obsidians overlap with the vesicular glasses. B. Notably, the obsidian clasts in the P2-P5 deposits mostly agree well with their vesicular counterparts (shown in dotted region).

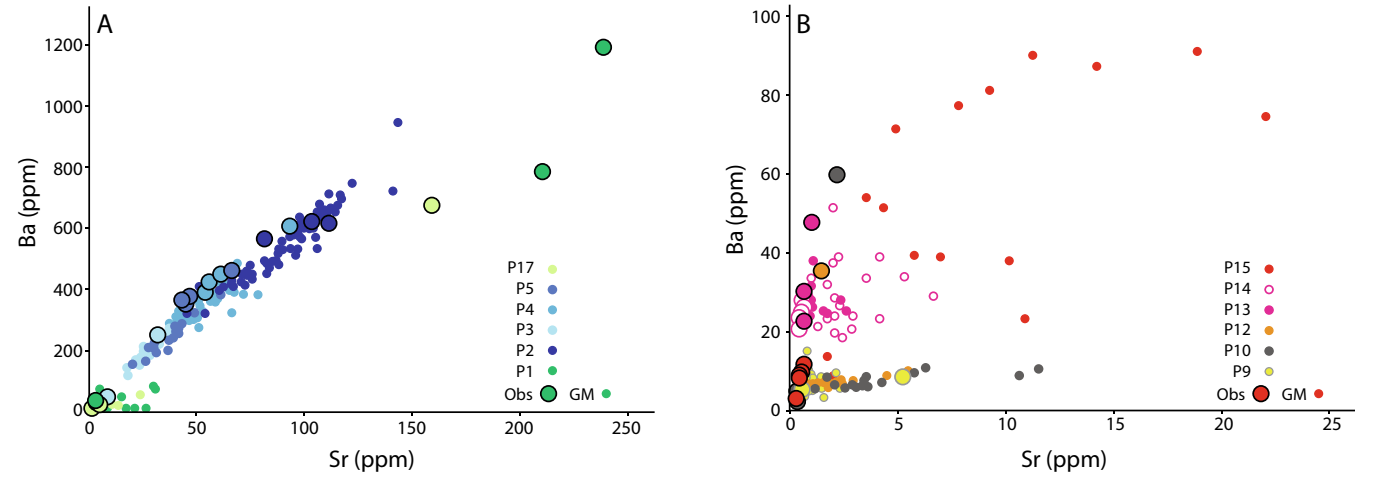

Fig. 6. Trace elemental compositions of the obsidian clasts (large symbols) and the groundmass glasses (small symbols) from the same tephras. Obsidian clast compositions are shown as the average composition of multiple measurements per clast. Data are separated into two diagrams as a function of trace elemental abundance (A. high abundance, B. low abundance). The majority of obsidian clasts have compositions that are consistent with their origin as juveniles while a few exceptions (P1, P10, P12, P15, and P17) have different compositions.

5. Discussion

5.1. Compositional relationships

Obsidian clasts may be genetically related to the co-erupted vesicular magma (i.e. juvenile) or they may be externally sourced and so considered as lithics (Fig. 7). Geochemically fingerprinting the obsidians remains the most reliable method of establishing whether the obsidian clasts are juvenile or not, yet this fundamental step remains often overlooked. Where the clasts are sufficiently large they may be analysed for bulk compositions and in some cases (e.g. the case of P13, above) this approach has been successful. However, using bulk compositions may be complicated if the mechanisms controlling obsidian formation involve physical processes such as fragmentation, mixing, and sintering that may occur multiple times in the shallow conduit (e.g., Gardner et al., 2017; Monnereau et al., 2021). In such cases, bulk rock compositions can be diverted away from magmatic compositions by crystal addition or subtraction. Thus, there is the potential for 'false negatives' in terms of defining the origin of an obsidian clast. In the case of the trachytic Pepom tephra deposits, with feldspar being the overwhelming mineral phase, it is an obvious candidate to be involved in modifying original compositions. Such processes would mimic those of cumulate entrainment in bulk compositions (e.g. Wolff et al., 2015). While obsidian clasts 1–3 in P15 (Fig. 4D) are notably higher in Ba (112–207 ppm) than the P15 pumice (28 ppm) other elements do not support a role for feldspar accumulation in these obsidian clasts as the average P15 feldspar is not sufficiently rich in Sr to explain the obsidian compositions. Similarly, a number of major and trace elements that are essentially absent in feldspar (e.g., MgO, MnO, Zr, Nb) are not lower in the obsidians than the pumice as would be expected if feldspar addition were occurring (Fig. 4D). These relationships suggest that the obsidian clasts 1–3 in P15 are unlikely to be sourced from the magma with which they co-erupted.

An alternative approach, which circumvents the issues of crystal accumulation / loss, is to compare the glass compositions found in the obsidians to that found in pumice clasts. Monnereau et al. (2021) found that the trace elemental composition of glasses in obsidians from the

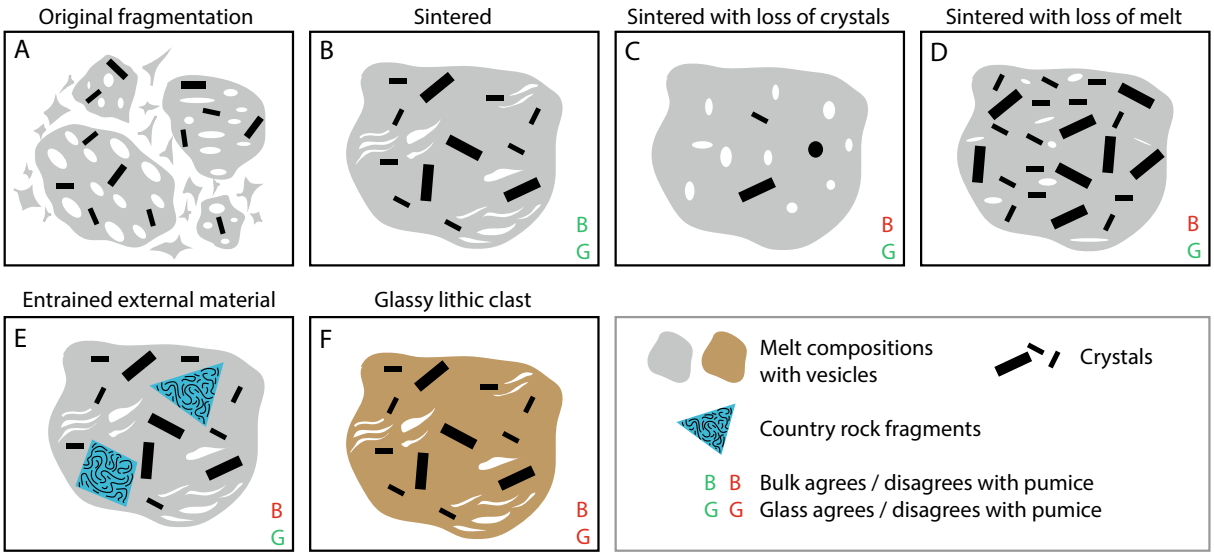

Fig. 7. Schematic of different types of obsidian and the geochemical information that they preserve. A. Initial fragmentation products. B. Sintering occurs without significant loss of components - bulk and glass compositions of obsidian are identical to pumices. Vesicle shapes are defined by the strain history in the shallow conduit, *interpretation - juvenile.* C. Sintering occurs with preferential accumulation of glass particles - bulk compositions diverted from pumices, *interpretation - juvenile.* D. Sintering occurs with preferential loss of glass particles - bulk compositions diverted from pumices towards cumulates, *interpretation - juvenile.* E. Fracturing of material in the shallow conduit causes ingress of country rock fragments - glass compositions of obsidian match those of pumice in the same deposit but bulk compositions are polluted by country rock involvement, *interpretation – compromised juvenile.* F. Entrainment of other glassy material from the shallow subsurface, glass compositions of obsidian do not match those of pumice in the same deposit, *interpretation – lithic.*

Snake River Plain had no relationship to the crystallinity of the obsidian clast, strongly supporting the model of physical mixing of components prior to the final formation (sintering) of the individual obsidian clast. This mechanical mixing is not restricted to the crystal cargo of the eruption and extraneous clasts can equally be engulfed within the sintering mass (scenario E in Fig. 7). While such hybrid juvenile-lithic clasts were not found within the Pepom tephras they have been seen in other obsidian bearing deposits (e.g. Fig. 9a of Monnereau et al., 2021 illustrating a clast within a clast). Due to this potential for mixing within the conduit the trace elemental compositions of glasses provide a particularly useful method to determine the origin of the material. Using the in-situ trace element data we interpret that from the Pepom tephra deposits ~71% (42/59) of the obsidian clasts as having compositions that are consistent with them being juvenile components. By combining both bulk and in-situ analyses we can learn more about the processes involved in obsidian formation. In the case of P13 where the bulk obsidian compositions are in excellent agreement with the pumice compositions, the in-situ compositions also highlight that the glasses are the same composition, further confirming their juvenile nature. This indicates that the processes involved in the formation of P13 obsidians do not involve significant mechanical mixing, or removal of materials (scenario B in Fig. 7).

With a sufficiently large dataset of in-situ and bulk analyses, it becomes apparent that, despite overall having rather similar appearances, individual deposits have their own specific characters in terms of obsidian sources. For example, within the P15 unit none of the 9 obsidian clasts investigated by in-situ methods returned compositions the same as the vesicular component of that eruption (scenario F in Fig. 7). This conclusion is further supported by the lack of agreement in bulk compositions between P15 obsidians and pumices (Fig. 6). This finding highlights that studies using dense pyroclasts to make inferences about conduit processes of specific eruptions are strengthened when the dense clasts can be independently shown to relate to the co-erupted vesicular magma, either via geochemistry or some other techniques.

5.2. Textural relationships

As noted above, there exists a huge amount of textural variability within the Pepom obsidian clasts (Fig. 3) both within single clasts and across clasts from a single deposit. What is particularly striking is the range in textures observed from clasts that are compositionally identified as juvenile. This relationship is in good agreement with previous works on obsidian formation that invoke physical processes of sintering as the cause for the textural variability within a suite of obsidian clasts, with each clast experiencing an individual history depending on the initial material sintered and its relative position in the conduit (Gardner et al., 2017; Wadsworth et al., 2020, 2022). The textures are remarkably similar to the range of vesicle textures documented in obsidian clasts from Mono Craters by Gardner et al. (2017). The variability preserved in vesicularity within a clast suggests that the material originally sintered was polymodal in grain size following the experimental results of Gardner et al. (2019). While the variation in bubble morphologies ranging from stretched, to distorted, to spherical reflect the progressive effects of surface tension relaxing the bubbles from initially irregular shapes towards spherical.

5.3. External obsidian sources

Although the majority of the obsidian clasts from the Pepom tephras as a whole have compositions consistent with their being juvenile, a minority are interpreted as being lithics and therefore require an additional source of material. One obvious potential source would be previously erupted products that were eroded and entrained during explosive eruptions. A possibility is that some of these obsidian clasts come from older pyroclastic deposits, such as the Bretanha and Santa Bárbara formations, which have abundant obsidian within their deposits (Queiroz et al., 2015). However, the pumices of the Santa Bárbara Formation have distinct and less evolved bulk rock compositions when compared to the Pepom tephras (Ellis et al., 2022, Fig. 4B). This is also the case for the juvenile materials of the Bretanha Formation, which are clearly less evolved than the Pepom tephra deposits (Queiroz et al., 2015). In contrast to many silicic volcanoes globally, there are no

obsidian lava bodies (domes or coulees) known to exist on the island of São Miguel. There are, however, some remains of domes in the southern part of Sete Cidades caldera, particularly in the vicinity of lake Verde – see Fig. 1 for location – (also Fig. 3 of Queiroz et al., 2008), which may have had bands of obsidian within the crystalline groundmass. In fact, we note that Queiroz et al. (2008) assigns the cone west of lake Verde as the vent for the P15 eruption. This is consistent with the observation that the P15 obsidians in both bulk rock and in-situ compositions are distinct from the co-erupted pumices (Figs. 4D and 6). Likewise, the P1 and P9 eruptions were also probably sourced from the lake Verde area (Queiroz et al., 2008) and while P1 has a dense clast that is not juvenile, those from P9 have juvenile compositions (see supplementary data). This highlights that the production of obsidian and the interaction with external lithologies varies on an eruption-by-eruption basis.

5.4. Controls on obsidian formation

While obsidian lavas are absent on the island of São Miguel, numerous domes and coulees with large bands of obsidian cutting through the crystalline groundmass are found on the neighbouring island of Terceira (Self and Gunn, 1976; Mungall and Martin, 1994, 1996). This allows us to evaluate potential controls on the formation of obsidian between these two islands in a similar geodynamic setting. The lava bodies with obsidian on Terceira are commonly present on the two active central volcanoes of the island (Fig. 9). The Pico Alto volcano is characterized by a large cluster of domes and coulees that completely fill and overflow an inconspicuous caldera, while the Santa Bárbara volcano, corresponds to a conical edifice with two small, overlapping summit calderas that are filled with domes. The flanks of Santa Bárbara also exhibit several alignments of domes and coulees (Self, 1976; Pimentel et al., 2016).

The Terceira silicic lavas are comenditic to pantelleritic in composition (Self and Gunn, 1976; Pimentel, 2006) and so differ significantly from the trachytes that represent the most evolved magmas on São Miguel (e.g., Beier et al., 2006; Jeffery et al., 2016; Ellis et al., 2022; Sup Fig. 3). While both Terceira systems are peralkaline (Fig. 9), the Pico Alto bulk rock compositions reach a peralkalinity (that is the (Na + K)/Al molar ratio) of nearly 1.8, while those from Santa Bárbara are slightly above 1.2 (Fig. 8). Increase in the peralkalinity index of a melt is promoted by the fractionation of phases with Al significantly in excess over alkalis, typically this is mostly achieved via feldspar removal (Bowen, 1945; Bailey and Schairer, 1964). The efficiency of the increase in

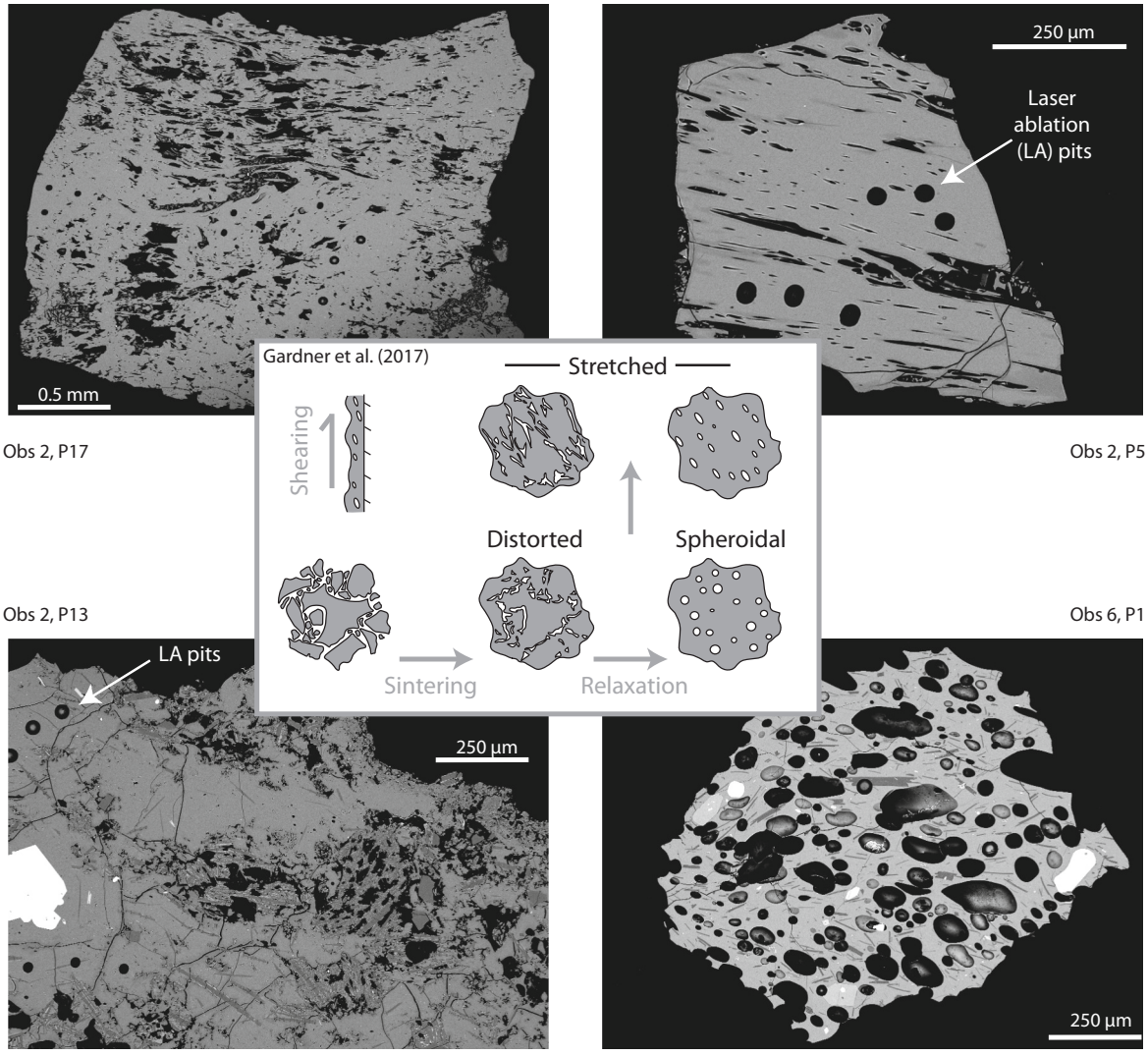

Fig. 8. Comparison of obsidian textures observed in backscatter electron images from the Pepom tephras with those observed by Gardner et al. (2017) from Mono Craters. The differing time-temperature-strain histories of the small parcels of melt produce the myriad of textures observed with the arrows indicating the progress of the process. The schematic diagram in the centre reflects the changing textures within an obsidian clast as a function of time relaxing the initially irregular vesicles towards spherical and how such vesicle types appear following shearing. Geochemical data illustrate that this variability of obsidian textures is due to the ascent of magma within the volcanic conduit.

peralkalinity is a function of the feldspar that is being removed with the more anorthitic feldspars most efficient at driving peralkalinity up. Peralkaline magmas are well-established to have lower viscosities than their metaluminous counterparts (e.g., Di Genova et al., 2013) and as such there is the intriguing possibility that the physical expression of the recent volcanism on Terceira, that is the production of domes / coulees (with large obsidian domains), could be modulated by deeper processes occurring early in the magmatic evolution. The sintering process is primarily controlled by the viscosity of the melt phase (itself a product of inter-related controls of composition, temperature, and volatile content) with additional factors involved such as particle size, crystal content, and particle shape amongst others (Gardner et al., 2018; Ryan et al., 2020; Wadsworth et al., 2022; Weaver et al., 2022). If compositional controls were playing an important role, we would expect the melts from Terceira, that sintered more efficiently producing obsidian in the lavas, to have a lower viscosity than those from Sete Cidades. To test this in a simplistic first order way, we can take compositions from each location and map melt viscosities across plausible temperature and water content space using the viscosity model of Giordano et al. (2008).

We highlight here that such an exercise requires a number of assumptions. Firstly, we assume that the initial particle size distribution was similar in the two sample suites. Secondly, we assume that the pyroclasts about to sinter in the conduit have relatively low water contents (typically <0.5 wt%) as most of the magmatic water is lost during magmatic fragmentation (Giachetti et al., 2015; Seligman et al., 2016) and thirdly we assume that the temperatures in the conduit are approximately similar. The temperature and water content assumptions are reasonable because geochemical investigations suggest that the Pepom magmas (789 ± 23 °C to 894 ± 20 °C and mostly 3–6 wt% H_2O, Ellis et al., 2022) and the Pico Alto magmas (850–900 °C uncertainty quoted as ±23 °C and 3–5.5 wt% H_2O, Jeffery et al., 2016) were stored under similar magmatic conditions. As can be seen from the viscosity maps in Fig. 9, the viscosities of the Terceira melts are systematically about half a log unit lower than those from Sete Cidades and as such are more likely to sinter under a given set of conditions. Interestingly however, the Pico Alto lavas with higher peralkalinity and consequently lower viscosity have less obsidian than the Santa Bárbara silicic lavas (our field observations). This implies that while large-scale compositional controls clearly have a role to play in determining the likelihood of obsidian formation via sintering other factors must be involved.

We can test this further by comparing sample P13 (Sete Cidades) with Terceira samples TERS 88 from Pico Alto, and TERS 70 from Santa Bárbara and computing the sintering timescales. To do this, we assume that the sintering occurred in the capillary regime where the densification on deposition from particles to obsidian was driven by the minimisation of internal surfaces via capillary flow. This was shown to be the likely regime for in-conduit sintering and sintering in most ignimbrites (excepting those with very high deposition rates; Wadsworth et al., 2019). In this regime, the time required for complete sintering is given by $\lambda = \mu R/\Gamma$, where μ is the average viscosity of the sintering clasts (Pa / s), R is the clast radius (μm), and Γ is the melt-vapour interfacial tension (N/m). Here, for comparison purposes, we select $R = 10\,\mu m$ and $\Gamma = 0.22$ N/m (after Gardner and Ketcham, 2011), and μ is dependent on temperature via the model by Giordano et al. (2008); discussed above and in Fig. 9). Using this scaling, we can compute λ as a function of temperature for P13 and for TERS 88 and TERS 70 at end-members of 0.1 and 1 wt% H_2O (Fig. 10). We find that indeed for a given temperature (e.g. the estimated temperature end members of 780 and 894 °C)

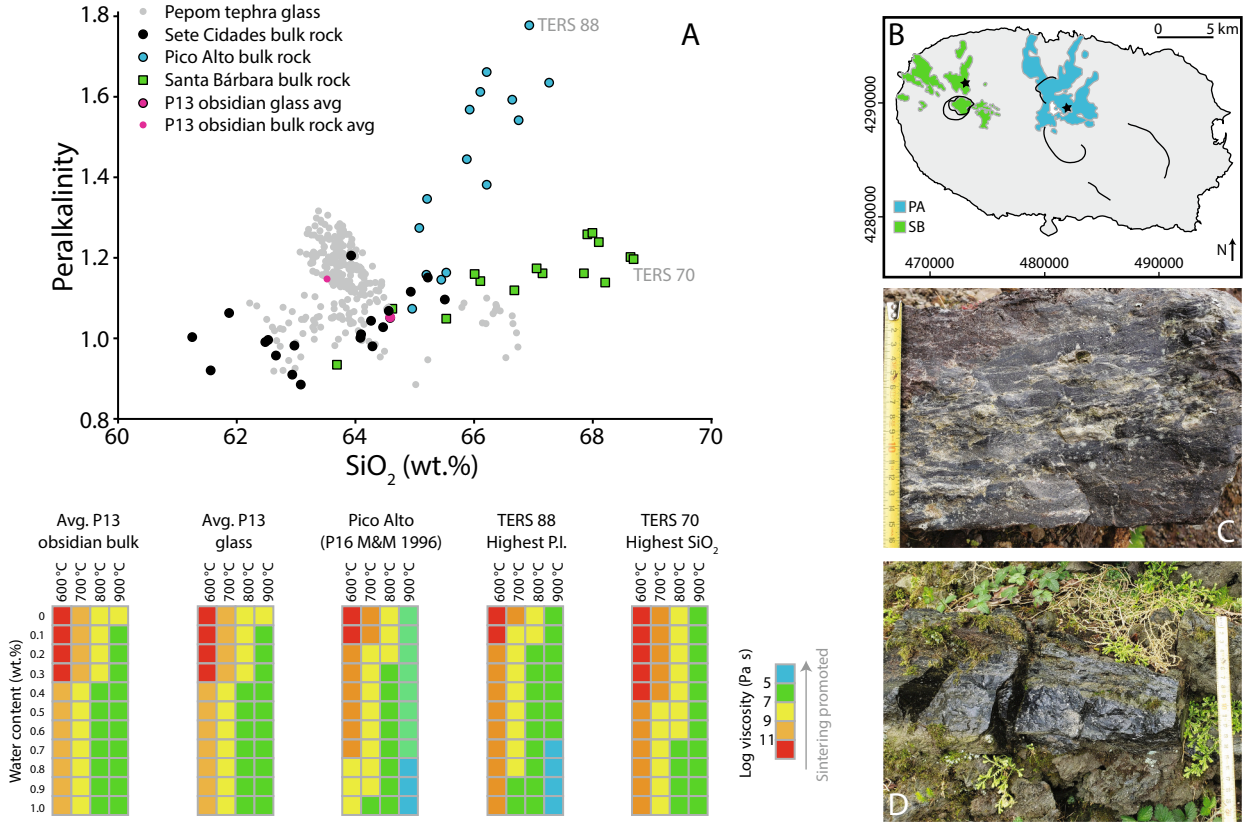

Fig. 9. Comparison of Sete Cidades and Terceira compositions. A. Diagram showing the range in peralkalinity between the evolved magmas of Sete Cidades (Ellis et al., 2022) and those from Pico Alto and Santa Bárbara on Terceira (Pimentel, 2006). Bottom panels: Comparison of the viscosity of Sete Cidades and Terceira compositions at conditions (600–900 °C and < 1 wt% H_2O) likely to be prevailing at in-vent sintering. Sample P16 (Pico Alto) from Mungall and Martin (1996); Samples TERS 70 (Santa Bárbara) and TERS 88 (Pico Alto) from Pimentel (2006). B. Simplified geological map of Terceira showing the distribution of the Pico Alto (PA) and Santa Bárbara (SB) silicic lavas (after Pimentel, 2006). C. Obsidian from Pico Alto. D. Obsidian from Santa Bárbara.

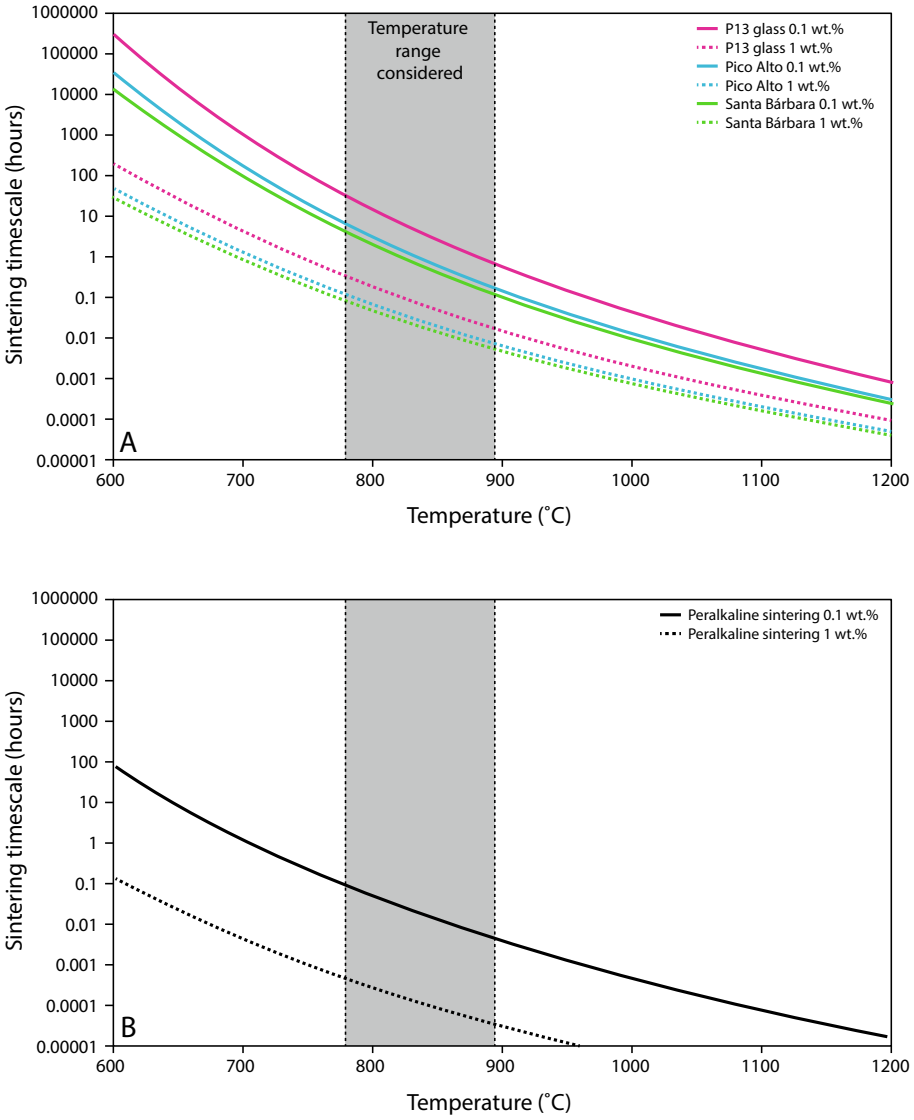

Fig. 10. The sinterability of the Sete Cidades and Terceira compositions cast as sintering timescale (in hours) as a function of temperature. In the sintering time calculation we use viscosity computed via (A) Giordano et al. (2008) and (B) Di Genova et al. (2013). The former is dependent on the composition, while the latter is a general model specifically calibrated for peralkaline compositions and is not dependent on the specific composition. In (A), for Terceira we use bulk compositions (Pimentel, 2006) while for Sete Cidades we use the P13 glass however as shown in Ellis et al. (2022) and in Fig. 9, the Sete Cidades bulk and glass compositions approximate each other. We use a reference particle size of 10 μm and assuming an interfacial tension of 0.22 N/m (Gardner and Ketcham, 2011).

the higher peralkalinity, and therefore lower viscosity, of the Terceira samples confers a lower sintering timescale compared with the Sete Cidades material. At 894 °C and 1 wt% H_2O the Sete Cidades material would sinter to dense obsidian in approximately 1 min, compared with 20–24 s for the Terceira material. This is clearly a lower bound on the sintering times given that this is the highest temperature and highest H_2O content considered. At the lower H_2O content of 0.1 wt%, the Sete Cidades material would sinter in just over 30 min, compared with 6–9 min for the Terceira material. If instead we assume the lower temperature of 780 °C, then the sintering time ranges move up to a range from minutes (e.g. Terceira sample TERS 88 at 1 wt% H_2O) to tens of hours (e.g. Sete Cidades sample P13 at 0.1 wt% H_2O). Fig. 10 demonstrates that the effect of peralkalinity between Pico Alto and Santa Bárbara is less significant in terms of sintering times that the effect of temperature and of H_2O content and therefore of degassing effects. Nevertheless, even with all of the uncertainties on these values, it is clear that there are striking differences in the sinterability between the Sete Cidades and the Terceira obsidians which are captured by this simple sintering timescale scaling.

We acknowledge that the Giordano et al. (2008) viscosity model is best calibrated for calc-alkaline compositions and the viscosity predictions for peralkaline compositions may be inaccurate. To test this, we also show the sintering timescale λ calculation using the viscosity model by Di Genova et al. (2013) calibrated specifically for peralkaline melts. This model is not composition dependent and as such there is a single model curve for 0.1 wt% H_2O and 1 wt% H_2O, respectively. Because this represents the high-peralkalinity limit of viscosity, the sintering timescales computed using the Di Genova et al. (2013) model are ubiquitously lower than those computed using the composition-dependent Giordano et al. (2008) model (compare Fig. 10b with Fig. 10a). At the temperature range used above, the 1 wt% H_2O sintering timescale is extremely rapid between 1 and 3 s, effectively instantaneous in the context of conduit-margin sintering. By contrast, at the lower 0.1 wt% H_2O, the predicted sintering timescale is between 30 s and 6 min, depending on the temperature.

The predominance of non-welded pyroclastic deposits with hydromagmatic characteristics within the Pepom Member at Sete Cidades has been attributed to the interaction of magma with external water from the caldera lakes playing a role in enhancing explosivity (Cole et al., 2008; Queiroz et al., 2008, 2015). The rapid cooling of particles during water-assisted fragmentation acts against sintering in the conduit, consistent with the volumetrically limited proportions of obsidians within the Pepom tephras. On Terceira, the Pico Alto record exhibits a temporal shift whereby the older stratigraphy is dominated by pyroclastic deposits while the younger record predominantly contains silicic lavas (Self, 1976; Gertisser et al., 2010) of broadly similar compositions.

The Pico Alto pyroclastic deposits include welded ignimbrites that are unlikely to have experienced water-assisted fragmentation (Gertisser et al., 2010; Pimentel et al., 2021) and so the change in eruptive style from explosive (pumice-forming) to effusive (obsidian-forming) cannot be attributed here to interaction with external water.

From the Azorean examples it is clear that sintering and the production of obsidian is the result of a complex interplay of processes that control the time-temperature history of pyroclasts within the shallow conduit. At depth these processes include those in the crustal magmatic system that define the evolutionary trajectory of the magmas and the resultant melt composition. In the conduit the timings of pyroclast-pyroclast interaction are controlled by a combination of the magmatic ascent rate, conduit dimensions, geometry and crystallinity amongst others (Watkins et al., 2017; Schipper et al., 2021; Wadsworth et al., 2020). Finally, external factors such as the rapid cooling of magma upon interaction with external water will act to diminish the ability of the clasts to sinter. Experimental studies are making great progress in isolating specific parameters to understand their importance (e.g. Gardner et al., 2018, 2019) and our combined field and geochemical studies complement these findings by defining the relationships between obsidian clasts and their co-erupted juvenile components.

6. Conclusions

The main conclusions of our study are:

1) Dense glassy clasts are common in the explosive eruptive products of the Sete Cidades volcano, both in the younger Pepom tephra deposits and also in the older deposits of the Bretanha and Santa Bárbara formations (Queiroz et al., 2015). The dense glassy clasts in these deposits commonly occur with pumiceous materials and they are found regardless of the extent of water-magma interaction inferred.

2) Strongly contrasting textural domains occur within single dense, glassy clasts. These textural domains may vary in vesicularity, groundmass crystallinity and phenocryst content. The contacts between such domains are typically irregular.

3) Commonly, the obsidian glass compositions overlap with the pumiceous glass compositions from the same deposit indicating that these differing clasts types are genetically linked.

4) Some deposits have very specific characters, for example P15 has no juvenile obsidian clasts based on either in-situ or bulk analyses. This highlights that it cannot be assumed in the absence of supporting evidence that obsidian clasts are related to the juvenile materials with which they are found.

5) São Miguel lacks obsidian lavas, but domes and coulees with large obsidian bands are found at the neighbouring island of Terceira, where the magmas are more strongly peralkaline. While magmatic processes may be acting to enhance peralkalinity, lower resultant viscosity, and enhance the likelihood of sintering, the greater abundance of obsidian in Santa Bárbara lavas (the less peralkaline suite) than in Pico Alto (both on Terceira) argues that conduit processes are a stronger control on obsidian formation.

Supplementary data to this article can be found online at https://doi.org/10.1016/j.chemgeo.2023.121694.

Declaration of Competing Interest

The authors declare the following financial interests/personal relationships which may be considered as potential competing interests:

Ben Ellis reports financial support was provided by Swiss National Science Foundation.

Data availability

All data are available in supplementary materials

Acknowledgements

We gratefully acknowledge financial support from the Swiss National Science Foundation (200020_197040 to BE). We thank Andreas Etter for help with sample preparation and Sebastian Ellis for hammering enthusiasm. Analytical work at ETH was facilitated by the customary excellence of Marcel Guillong and Lydia Zehnder. We would like to thank Silvio Mollo and Alessandro Vona for reviews that improved this work and Claudia Romano for editorial handling.

References

Bachmann, O., Charlier, B.L.A., Lowenstern, J., 2007. Zircon crystallization and recycling in the magma chamber of the rhyolitic Kos Plateau Tuff (Aegean arc). Geology 35, 73–76.

Bailey, D.K., Schairer, J.F., 1964. Feldspar-liquid equilibria in peralkaline liquids; the orthoclase effect. Am. J. Sci. 262, 1198–1206.

Barnes, J.D., Prather, T.J., Cisneros, M., Befus, K., Gardner, J.E., Larson, T.E., 2014. Stable chlorine isotope behavior during volcanic degassing of H_2O and CO_2 at Mono Craters, CA. Bull.Volcanol. 76, 805.

Beier, C., Haase, K.M., Hansteen, T.H., 2006. Magma evolution of the Sete Cidades volcano. São Miguel. Azores. J. Petrol. 47, 1375–1411. https://doi.org/10.1093/petrology/egl014.

Beier, C., Haase, K.M., Turner, S.P., 2012. Conditions of melting beneath the Azores. Lithos 144–145, 1–11.

Bowen, N.L., 1945. Phase equilibria bearing on the origin and differentiation of the alkaline rocks. Amer. J. Sci. 243A, 75–89.

Cannat, M., Briais, A., Delpus, C., Escartin, J., Georgen, J., Lin, J., Mercouriev, S., Meyzen, C., Muller, M., Pouliquen, G., Rabain, A., da Silva, P., 1999. Mid-Atlantic Ridge–Azores hotspot interactions: along-axis migration of a hotspot-derived event of enhanced magmatism 10 to 4 Ma ago. Earth Planet. Sci. Lett. 173, 257–269.

Carmo, R., Madeira, J., Ferreira, T., Queiroz, G., Hipólito, A., 2015. Volcanotectonic structures of São Miguel Island, Azores. In: Gaspar, J.L., Guest, J.E., Duncan, A.M., Barriga, F.J.A.S., Chester, D.K. (Eds.), Volcanic Geology of São Miguel Island (Azores Archipelago), Geological Society, London, Memoirs, 44, pp. 65–86. https://doi.org/10.1144/M44.6.

Castro, J.M., Bindeman, I.N., Tuffen, H., Schipper, C.I., 2014. Explosive origin of silicic lava: Textural and δD–H_2O evidence for pyroclastic de- gassing during rhyolite effusion: Earth and Plan. Sci.Lett. 405, 52–61.

Cole, P.D., Pacheco, J.M., Gunasekera, R., Queiroz, G., Goncalves, P., Gaspar, J.L., 2008. Contrasting styles of explosive eruption at Sete Cidades, São Miguel, Azores, in the last 5000 years: Hazard implications from modelling. J. Volcanol. Geotherm. Res. 178, 574–591.

Di Genova, D., Romano, C., Hess, K.U., Vona, A., Poe, B.T., Giordano, D., Dingwell, D.B., Behrens, H., 2013. The rheology of peralkaline rhyolites from Pantelleria Island. J. Volcanol. Geotherm. Res. 249, 201–216.

Donovan, J.J., Tingle, T.N., 1996. An improved mean atomic number background correction for quantitative microanalysis. Microsc. Microanal. 2 (1), 1–7.

Donovan, J.J., Singer, J.W., Armstrong, J.T., 2016. A new EPMA method for fast trace element analysis in simple matrices. Am.n Mineral. 101 (8), 1839–1853.

Donovan, J., Kremser, D., Fournelle, J., Goemann, K., 2018. Probe for Windows User's Guide and Reference, Enterprise edition. Probe Software, Inc, Eugene, Oregon.

Ellis, B.S., Pimentel, A., Wolff, J.A., Etter, A., Cortes-Calderon, E.A., Harris, C., Mark, D. F., Neukampf, J., Bachmann, O., 2022. Geochemistry of the Pepom tephra deposits: the most recent intracaldera volcanism of Sete Cidades volcano, São Miguel. Azores. J. Volcanol. Geotherm. Res 432, 107673.

Gardner, J.E., Ketcham, R.A., 2011. Bubble nucleation in rhyolite and dacite melts: temperature dependence of surface tension. Contrib. Mineral. Petrol. 162, 929–943.

Gardner, J.E., Llewellin, E.W., Watkins, J.M., Befus, K.S., 2017. Formation of obsidian pyroclasts by sintering of ash particles in the volcanic conduit. Earth Planet. Sci. Lett. 459, 252–263.

Gardner, J.E., Wadsworth, F.B., Llewellin, E.W., Watkins, J.M., Coumans, J.P., 2018. Experimental sintering of ash at conduit conditions and implications for the longevity of tuffisites. Bull. Volcanol. 80, 23.

Gardner, J.E., Wadsworth, F.B., Llewellin, E.W., Watkins, J.M., Coumans, J.P., 2019. Experimental constraints on the textures and origin of obsidian pyroclasts. Bull. Volcanol. 81, 22.

Gertisser, R., Self, S., Gaspar, J.L., Kelley, S.P., Pimentel, A., Eikenberg, J., Barry, T.L., Pacheco, J.M., Queiroz, G., Vespa, M., 2010. Ignimbrite stratigraphy and chronology on Terceira Island, Azores. In: Groppelli, G., Viereck-Goette, L. (Eds.), Stratigraphy and geology of volcanic areas, Geological Society of America, Special Paper, 464, pp. 133–154. https://doi.org/10.1130/2010.2464(07).

Giachetti, T., Gonnermann, H.M., Gardner, J.E., Shea, T., Gouldstone, A., 2015. Discriminating secondary from magmatic water in rhyolitic matrix-glass of volcanic pyroclasts using thermogravimetric analysis. Geochim. Cosmochim. Acta 148, 457–476.

Giordano, D., Russell, J.K., Dingwell, D.B., 2008. Viscosity of magmatic liquids: a model. Earth Planet. Sci. Lett. 271, 123–134.

Guest, J.E., Gaspar, J.L., Cole, P.D., Queiroz, G., Duncan, A.M., Wallenstein, N., Ferreira, T., Pacheco, J.M., 1999. Volcanic geology of Furnas Volcano, São Miguel, Azores. J. Volcanol. Geotherm. Res. 92, 1–29. https://doi.org/10.1016/S0377-0273(99)00064-5.

Guillong, M., Meier, D., Allan, M., Heinrich, C., Yardley, B., 2008. Laser Ablation ICP–MS in the Earth Sciences: Current Practices and Outstanding Issues. Mineralogical Association of Canada, Canada, pp. 328–333.
Hansteen, T.H., Klugel, A., Schmincke, H.U., 1998. Multi-stage magma ascent beneath the Canary Islands:evidence from fluid inclusions. Contrib. Mineral.Petrol. 132, 48–64.
Hildreth, W., Mahood, G.A., 1986. Ring-fracture eruption of the Bishop Tuff. Geol. Soc. Am. Bull. 97, 396–403.
Jeffery, A.J., Gertisser, R., O'Driscoll, B., Pacheco, J.M., Whitley, S., Pimentel, A., Self, S., 2016. Temporal evolution of a post-caldera, mildly peralkaline magmatic system: Furnas volcano, São Miguel. Azores. Contrib. Mineral. Petrol. 171, 42.
Kueppers, U., Pimentel, A., Ellis, B., Forni, F., Neukampf, J., Pacheco, J., Perugini, D., Queiroz, G., 2019. Biased Volcanic Hazard Assessment due to Incomplete Eruption Records on Ocean Islands: An Example of Sete Cidades Volcano. Frontiers in Earth Science, Azores. https://doi.org/10.3389/feart.2019.00122.
Laeger, K., Petrelli, M., Morgavi, D., Lustrino, M., Pimentel, A., Paredes-Mariño, J., 2019. Pre-eruptive conditions and triggering mechanism of the _16 ka santa bárbara explosive eruption of sete cidades volcano (São Miguel. Azores). Contrib. Mineral. Petrol. 174, 11. https://doi.org/10.1007/s00410-019-1545-y.
Métrich, N., Zanon, V., Creon, L., Hildenbrand, A., Moreira, M., 2014. Is the 'Azores hotspot'a wetspot? Insights from the geochemistry of fluid and melt inclusions in olivine of Pico basalts. J. Petrol. 55, 377–393.
Monnereau, L.R., Ellis, B.S., Szymanowski, D., Bachmann, O., Guillong, M., 2021. Obsidian pyroclasts in the Yellowstone-Snake River Plain ignimbrites are dominantly juvenile in origin. Bull. Volcanol. 83, 27.
Moore, R., 1990. Volcanic geology and eruption frequency. São Miguel. Azores. Bull. Volcanol. 52, 602–614. https://doi.org/10.1007/BF00301211.
Mungall, J.E., Martin, R.F., 1994. Severe leaching of trachytic glass without devitrification, Terceira, Azores. Geochim. Cosmochim. Acta 58, 75–83. https://doi.org/10.1016/0016-7037(94)90447-2.
Mungall, J.E., Martin, R.F., 1996. Extreme differentiation of peralkaline rhyolite, Terceira, Azores; a modern analogue of Strange Lake, Labrador? Can. Mineral. 34, 769–777.
Newman, S., Epstein, S., Stolper, E., 1988. Water, carbon dioxide, and hydrogen isotopes in glasses from the ca. 1340 A.D. eruption of the Mono Craters, California: Constraints on degassing phenomena and initial volatile content. J. Volcanol. Geotherm. Res. 35 (1–2), 75–96.
Pimentel, A., 2006. Domos e coulées da ilha Terceira (Açores): Contribuição para o estudo dos mecanismos de instalação. In: Tese de Mestrado em Vulcanologia e Riscos Geológicos. Universidade dos Açores, Departamento de Geociências, 143 pp. (in portuguese).
Pimentel, A., Zanon, V., De Groot, L.V., Hipólito, A., Di Chiara, A., Self, S., 2016. Stress-induced comenditic trachyte effusion triggered by trachybasalt intrusion: multidisciplinary study of the AD 1761 eruption at Terceira Island (Azores). Bull. Volcanol. 78, 1–21. https://doi.org/10.1007/s00445-016-1015-6.
Pimentel, A., Self, S., Pacheco, J.M., Jeffery, A.J., Gertisser, R., 2021. Eruption style, emplacement dynamics and geometry of peralkaline ignimbrites: Insights from the Lajes-Angra Ignimbrite Formation, Terceira Island. Azores. Front. Earth Sci. 9, 673686 https://doi.org/10.3389/feart.2021.673686.
Pittari, A., Cas, R.A.F., Wolff, J.A., Nichols, H.J., Larson, P.B., Marti, J., 2008. The Use of Lithic Clast Distributions in Pyroclastic Deposits to Understand Pre- and Syn-Caldera Collapse Processes: A Case Study of the Abrigo Ignimbrite, Tenerife, Canary Islands. Develop. Volcanol. 10, 97–142.
Porreca, M., Pimentel, A., Kueppers, U., Izquierdo, T., Pacheco, J., Queiroz, G., 2018. Event stratigraphy and emplacement mechanisms of the last major caldera eruption on Sete Cidades Volcano (São Miguel, Azores): the 16 ka Santa Bárbara Formation. Bull. Volcanol. 80, 76. https://doi.org/10.1007/s00445-018-1250-0.
Queiroz, G., 1997. Vulcão das Sete Cidades (S.Miguel, Açores): História Eruptiva e Avaliação do Hazard. Ph.D. Thesis,. Azores University, Portugal.
Queiroz, G., Pacheco, J.M., Gaspar, J.L., Aspinall, W.P., Guest, J.E., Ferreira, T., 2008. The last 5000 years of activity at Sete Cidades volcano (São Miguel Island, Azores): implications for hazard assessment. J. Volcanol. Geotherm. Res. 178, 562–573. https://doi.org/10.1016/j.jvolgeores.2008.03.001.
Queiroz, G., Gaspar, J.L., Guest, J.E., Gomes, A., Almeida, M.H., 2015. Eruptive history and evolution of Sete Cidades Volcano, São Miguel Island, Azores. In: Gaspar, J.L., Guest, J.E., Duncan, A.M., Barriga, F.J.A.S., Chester, D.K. (Eds.), Volcanic Geology of São Miguel Island (Azores Archipelago). Geological Society of London), (London, pp. 87–104. https://doi.org/10.1144/M44.7.
Rust, A.C., Cashman, K.V., 2007. Multiple origins of obsidian pyroclasts and implications for changes in the dynamics of the 1300 B.P. eruption of Newberry Volcano. USA. Bull. Volcanol. 69, 825–845.
Rust, A.C., Cashman, K.V., Wallace, P.J., 2004. Magma degassing buffered by vapor flow through brecciated conduit margins. Geology 32 (4), 349–352.
Ryan, A.G., Russel, J.K., Heap, M.J., Zimmerman, M.E., Wadsworth, F.B., 2020. Timescales of porosity and permeability loss by solid-state sintering. Earth Planet. Sci. Lett. 549, 116533.
Schipper, C.I., Castro, J.M., Kennedy, B.M., Tuffen, H., Whattam, J., Wadsworth, F.B., Paisley, R., Fitzgerald, R.H., Rhodes, E., Schaefer, L.N., Ashwell, P.A., Forte, P., Seropian, G., Alloway, B.V., 2021. Silicic conduits as supersized tuffisites: Clastogenic influences on shifting eruption styles at Cordón Caulle volcano (Chile). Bull. Volcanol. 83, 11.
Self, S., 1976. The recent volcanology of Terceira, Azores. J. Geol. Soc. Lond. 132, 645–666. https://doi.org/10.1144/gsjgs.132.6.0645.
Self, S., Gunn, B.M., 1976. Petrology, volume and age relations of alkaline and saturated peralkaline volcanics from Terceira, Azores. Contrib. Mineral. Petrol. 54, 293–313. https://doi.org/10.1007/BF00389409.
Seligman, A.N., Bindeman, I.N., Watkins, J.M., Ross, A.M., 2016. Water in volcanic glass: From volcanic degassing to secondary hydration. Geochim. Cosmochim. Acta 191, 216–238.
Taylor, B.E., Eichelberger, J.C., Westrich, H.R., 1983. Hydrogen isotopic evidence of rhyolitic magma degassing during shallow intrusion and eruption. Nature 306, 541–545.
Trippanera, D., Porreca, M., Ruch, J., Pimentel, A., Acocella, V., Pacheco, J., Salvatore, M., 2014. Relationships between tectonics and magmatism in a transtensive/transform setting: an example from Faial Island (Azores, Portugal). Geol. Soc. Am. Bull. 126, 164–181. https://doi.org/10.1130/B30758.1.
Troch, J., Ellis, B.S., Harris, C., Ulmer, P., Bachmann, O., 2018. The effect of prior hydrothermal alteration on the melting behaviour during rhyolite formation in Yellowstone, and its importance in the generation of low- $\delta^{18}O$ magmas. Earth Planet. Sci. Lett. 481, 338–349.
Tuffen, H., Farquharson, J., Wadsworth, F.B., Webb, C., Owen, J., Castro, J.M., Berlo, K., Schipper, C.I., Wehbe, K., 2022. Mid-loaf crisis: Internal breadcrust surfaces in rhyolitic pyroclasts reveal dehydration quenching. Geology 50, 1058–1062.
Turner, S., Tonarini, S., Bindeman, I.N., Leeman, W.P., Schaefer, B.F., 2007. Boron and oxygen isotope evidence for recycling of subducted components over the past 2.5 Gyr. Nature 447, 702–705. https://doi.org/10.1038/nature05898.
Wadsworth, F.B., Vasseur, J., Schauroth, J., Llewellin, E.W., Dobson, K.J., Havard, T., Scheu, B., von Aulock, F.W., Gardner, J.E., Dingwell, D.B., Hess, K.U., 2019. A general model for welding of ash particles in volcanic systems validated using in situ X-ray tomography. Earth Planet. Sci. Lett. 525, 115726.
Wadsworth, F.B., Llewellin, E.W., Vasseur, J., Gardner, J.E., Tuffen, H., 2020. Explosive-effusive volcanic eruption transitions caused by sintering. Sci, Adv, p. 6.
Vogt, P.R., Jung, W.Y., 2004. The Terceira Rift as hyper-slow hotspot dominated oblique spreading axis: a comparison with other slow-spreading plate boundaries. Earth Planet. Sci. Lett. 218, 77–90. https://doi.org/10.1016/S0012-821X(03)00627-7.
Wadsworth, F.B., Llewellin, E.W., Castro, J.M., Tuffen, T., Schipper, C.I., Gardner, J.E., Vasseur, J., Foster, A., Damby, D.E., McIntosh, I.M., Boettcher, S., Unwin, H.E., Heap, M.J., Farquharson, J.I., Dingwell, D.B., Iacovino, K., Paisley, R., Jones, C., Whattam, J., 2022. A reappraisal of explosive–effusive silicic eruption dynamics: syn-eruptive assembly of lava from the products of cryptic fragmentation. J. Volcanol. Geotherm. Res. 432, 107672.
Wang, Y., Gardner, J.E., Hoblitt, R.P., 2021. Formation of dense pyroclasts by sintering of ash particles during the preclimactic eruptions of Mt. Pinatubo in 1991. Bull. Volcanol. 83, 6.
Watkins, J.M., Gardner, J.E., Befus, K.S., 2017. Nonequilibrium degassing, regassing, and vapor fluxing in magmatic feeder systems. Geology 45, 183–186.
Weaver, J., Lavallee, Y., Ashraf, M., Kendrick, J.E., Lamur, A., Schauroth, J., Wadsworth, F.B., 2022. Vesiculation and densification of pyroclasts: A clast-size dependent competition between bubble growth and diffusive outgassing. J. Volcanol. Geotherm. Res. 428, 107550.
Wilson, C.J.N., Hildreth, W., 1997. The Bishop Tuff: New Insights From Eruptive Stratigrapgy. J. Geol. 105, 407–516.
Wolff, J.A., Ellis, B.S., Ramos, F.C., Starkel, W.A., Boroughs, S., Olin, P.H., Bachmann, O., 2015. Remelting of cumulates as a process for producing chemical zoning in felsic tuffs: a comparison of cool, wet and hot, dry silicic magma systems. Lithos 236–237, 275–286.